GROUND SURFACE EFFECTS IN WIND FARMS:

A MICRO WIND FARM MODEL STUDY

by

Yifan Zhang

A thesis submitted to the Johns Hopkins University in conformity with the requirements for the degree of Master of Science in Engineering

Baltimore, Maryland

January, 2018

Abstract

Roughness and obstacles on terrain can greatly influence the power output of a wind farm. In this essay, the effects of such surface roughness on a wind farm are explored using a micro wind farm model placed in a wind tunnel. Moreover, building upon recent studies that raised the possibility to increase power output by using windbreaks, the potential of windbreaks is also investigated by wind tunnel measurements. In this study porous disc models are used as a model for the wind turbines, allowing the measurement of the power output, thrust force and spatially averaged incoming velocity for every turbine. The model wind farm consists of 100 wind turbine models. Experimental results show that additional surface roughness can significantly reduce the total power output of a wind farm. Results also show that the negative impact of windbreak wakes for an aligned wind farm will outweigh the local inviscid speed-up and thus not provide increased power output.

Primary Reader: Charles Meneveau

Secondary Reader: Dennice Gayme

Acknowledgements

The experiments of this work were funded by the National Science Foundation (grant #OISE 1243482, the WINDINSPIRE project).

I am immensely grateful to Prof. C. Meneveau for his patient guidance throughout the research, as well as his persevering and careful amendments to the manuscripts of this essay. I would like to express my gratitude to Dr. J. Bossuyt for establishing a solid foundation for this research and providing assistance during the course of this research. I would also like to thank Prof. D. Gayme for her final amendments to this essay.

Special thanks go to the Johns Hopkins University for providing me with partial tuition support.

Contents

List of Figures

1. Introduction

Along with the development of the global economy, fulfilling the quickly increasing demand of energy is a major issue that humans are facing (Leung and Yang, 2012). In addition, conventional fossil fuels, such as coal, oil and natural gas, will eventually become scarce and have become a concern because of environmental disruption and climate change. Hence, there is an urgent need for capacity expansion of clean and renewable energy. Among many of the clean and renewable energies, such as solar, tidal and geothermal energy, wind energy is most technologically mature and thus has the most immediate promise in terms of commercial potential (Deal, 2010). In short, the growing popularity of wind energy and its trend of becoming one of the most profitable renewable energy sources bodes well for the its future (Ackermann and Söder, 2002). Still, further optimized and improved designs of wind farms are needed, which require a better understanding of the interaction between wind farms and the terrain under them. The local wind speed, as a major contributor to power output of wind turbines, is affected by the friction against the ground surface – upon which wind farms are built. When constructing wind farms on flat terrain, one has to account for the impact of different crops, forests, fencerows and buildings to maximize the local speed at every wind turbine. Wind tunnels have been used with great success since the dawn of aviation as a tool to engineer new concepts in

aerodynamics. While wind tunnel experiments have been widely used to study wind farms and associated fluid dynamics (Cal et al. 2010, Chamorro & Porté-Agel, 2009, Bossuyt et al. 2017), wind tunnel studies on how ground surface roughness affects the energy harvested by large wind farms have not been carried out yet.

1.1 Wind farm research using wind tunnel

The method of exploring wind farm performance, especially for wind turbine efficiency, by conducting wind tunnel experiments has been employed by a number of previous researchers. Surface inhomogeneities (roughness and topography) and thermal stratification are two important factors that influence the turbulent boundary layer, which is the lowest region of the atmospheric boundary layer (ABL). Since wind turbines operate in this region, they are affected by the same factors. Thermal stratification has been the focus of prior research of Zhang et al. (2013), who mainly focused on the effects of wind turbine wakes in a convective boundary layer. By changing the properties of the turbulent ABL, thermal stability affects the behavior of wind-turbine wakes.

To characterize forces acting on the turbine structure, the National Renewable Energy Laboratory (NREL) conducted the Unsteady Aerodynamics Experiment (UAE) (Simms et al., 2001). As part of that project, accurate

quantitative aerodynamic and structural measurements were conducted by Hand et al. (2001) on an extensively instrumented wind turbine in the giant NASA-Ames 24.4 m by 36.6 m cross-section wind tunnel, which is representative of now medium-scale turbine machines in both geometry and dynamics.

A combined result from wind tunnel tests and simulations helps to build better prediction models. Based on wind tunnel tests of model turbines (at NTNU Trondheim) with diameters of about ~0.9 m, a series of blind test calculations were made by researchers. A wide range of methods, such as standard Blade Element Momentum (BEM) and Large Eddy Simulation (LES), were used to predict the performance and the wake development for the model wind turbines (Krogstad & Eriksen, 2013; Pierella, 2014; Krogstad et al., 2015).

Blade loads and pressure distribution measurements as well as extensive PIV flow field measurements were conducted by Schepers et al. (2012) on a 4.5 m diameter wind turbine to validate and improve aerodynamic wind turbine models. Further comparison between additional wind tunnel tests and comparative CFD simulations was conducted by Schepers et al. (2014) as well as in follow-on research (see e.g. the review by Stevens & Meneveau, 2017).

Wind-tunnel experiments were performed to study turbulence in the wake of a model wind turbine by Chamorro and Porte-Agel (2009). In their research,

they placed a model wind turbine in a boundary layer developed over surfaces with different turbulence levels. Over both rough and smooth surfaces, they characterized the cross-sectional distribution of mean velocity, turbulence intensity and kinematic shear stress using hot-wire anemometry. Important factors affecting turbine power generation in wind farms such as the spatial distribution of the velocity deficit and the turbulence intensity were studied in particular. Further research on the instability mechanisms in wind turbine wakes using wind tunnel tests was conducted by Iungo (2015). In his study, wind tunnel velocity measurements of wakes produced by down-scaled wind turbine models were presented. The turbulence data acquired for a uniform incoming flow were used to predict the hub vortex instability observed in the near wake of a wind turbine.

The characteristics of unsteady loading and spatiotemporal power output in wind farms were demonstrated by wind tunnel measurements conducted by Bossuyt et al. (2017). A micro wind farm model composed of 3cm diameter porous disk wind turbine models was tested under multiple layouts in order to determine the turbine-to-turbine cross correlation of the power output.

None of studies stated above was focused on the ground surface roughness effects underlying wind farms. In the present study, we will use the same facility and wind turbine models as in the study of Bossuyt et al. (2017) to determine the

influence of multiple kinds of ground roughness situations on the resulting mean power output of the farm.

1.2 Roughness effects

The effects of roughness and roughness elements on the ABL have been studied for many years. For instance, Tani and Sato (1956) made measurements in the boundary layer along a flat plate placed in a low turbulence wind tunnel. They attached a fine rod to the plate as a two-dimensional roughness element and investigated the resulting transition from laminar to turbulent flow with hot-wire equipment. Blom (1969) specifically looked into the influence of changes in surface roughness on the development of the turbulent boundary layer in the lower layers of the atmosphere, which is where wind turbines operate. He described the development of an internal turbulent boundary layer in a neutral atmosphere downwind of an abrupt change in surface roughness. Meanwhile, a theory for predicting the variation of the wind profile as a function of surface roughness and stability was introduced by Irvin (1979) using the formulation of Nickerson and Smiley (1975) for specifying the vertical profile of horizontal wind velocity. Essa et al. (2003) made comparisons between various estimates of the power-law exponents from various sources. Ragheb (2012) explained how wind shear is related to different classes of surface roughness around wind

turbines and corresponding contributions to wind energy production potential at a given site. Chen et al. (2015) investigated and compared the behaviors of overland flow resistance from multi-scale configurations of different roughness elements. In their study, the decreasing vegetation density – only in spacing between individual vegetation rows – tended to reduce the flow resistance. Mattuella et al. (2015) utilized wind tunnel experiments to perform detailed analyses of complex terrain effects for wind turbine micrositing in a wind energy project. The combined use of wind tunnel and mesoscale numerical modeling represents an even better approach for wind power site assessment in a complex terrain. De Paepe et al. (2016) simulated the ABL over suburban terrain in an industrial-scale wind tunnel. In their study, two different Barrier Mixing Device (RBMD) methods for simulating the ABL were used, including the well-known combination of Counihan quarter ellipses and roughness elements and a new configuration based on truncated Irwin spires and roughness elements. Effects of roughness on the fundamental structure of turbulent boundary layers are reviewed in Jimenez (2004).

1.3 Windbreaks

The role that topography plays in the performance of a wind farm is undeniably an important one. There are many ways to artificially modify the

topography at a particular site. For example, agriculturalists have used windbreaks as an efficient way to modify the topography of farmlands for hundreds of years. Systematic generalization of windbreak application is difficult even though there have been many experiments applied to specific contexts. The interest in windbreaks arises due to their wide range of practical applications. Agriculture, forestry, soil conservation and wind farms are all potential target areas. (Judd et al., 1996). However, as we are still not able to reliably predict the aerodynamic performance of windbreaks, they remain a subject of active research, especially when applied to windfarms.

Tobin et al. (2017) recently proved that windbreaks are capable of diverting low-level flow to the level at wind turbine hub-height. In their study, the prediction that perturbed hub-height velocities may be able to increase power production by around 10% was corroborated with power-production measurements from a wind tunnel experiment using a single model turbine. Results showed that the net impact on power production is positive for short windbreaks, and negative for tall windbreaks. However, their study failed to predict windbreak effects on large wind farms where wake interactions are critical. Most recently, Tobin and Chamorro (2017) explored windbreak effects in a large wind farm using simplified analytical model formulations. The results of their study suggested that the negative impact of windbreak wakes for an infinite

wind farm will outweigh the local inviscid speed-up for realistic inter-turbine spacings. Only wind farms with wind turbine spacing of more than ~25 rotor diameters were expected to achieve higher power output due to wind breaks. However, physical experimental investigations are required to properly assess the net effects of windbreaks in large wind farms.

In the current study we use a wind tunnel physical experimental setup to quantify the effects of windbreaks in large windfarms. We make use of 100 porous disk models within a micro-scale wind farm to perform measurements of the power output of each turbine under multiple surface conditions, including the implementation of various levels of surface roughness as well as windbreaks. Among the 100 porous disk models, 60 are equipped with strain gages. For each of them, correlations between bending moment, thrust, wind velocity and power output are derived from the stain signal data collected as function of time. Polyester stripes are implemented among wind turbine model rows as roughness elements, and corrugated plastic sheet blocks are installed to mimic the function of windbreaks. This study provides an opportunity to understand the effects of ground roughness and windbreaks on wind farm performance using well-controlled wind tunnel experiments. Also, the results presented here are ideal for instructing the wind farm design initially focused on enhancing power efficiency. The set-up of the micro-scale wind-farm and measurement

capabilities are described in section 2 and section 3, respectively. Average row powers under various ground surface settings are studied in section 4.

2. Experimental set-up

This thesis makes use of the Stanley Corrsin Wind Tunnel at the Johns Hopkins University. This closed loop, two-storey facility has a test section of length of approximately 10m and a cross-sectional area of 0.9m by 1.2m. It has a primary contraction ratio of 25:1 and a secondary one of 1.27:1, which helps to develop a smooth inflow starting at the beginning of the test section. The cross-sectional area is designed to gradually increase downstream to compensate for wall boundary layer development. The background turbulence intensity is about $TI_u \approx 0.12\%$, which is relatively low. The boundary layer developing on the lower plate is tripped by three metal chains placed across the start of the test section and is allowed to develop naturally for 5 m before encountering the micro wind farm, as shown in Figure 1.

2.1 Porous disk wind turbine model

To enable building a large wind farm model with 100 wind turbine models in a relatively small wind tunnel test section, a porous disk model is adopted. It is conveniently small-sized, easily manufactured and reproduces wind turbine

wakes appropriately （Lignarolo et al., 2014; Bossuyt et al., 2017）. The model wind farm set-up to be used in the present experiments is shown schematically in Figure 1. After being tripped by the metal chains at the entrance of the test section, the boundary layer develops naturally through the first half of the wind tunnel. It reaches a height of $\delta_{99} = 0.18m$ at the front end of the model wind farm, which corresponds to 4.5 times the porous disk top-height. (Bossuyt et al., 2017)

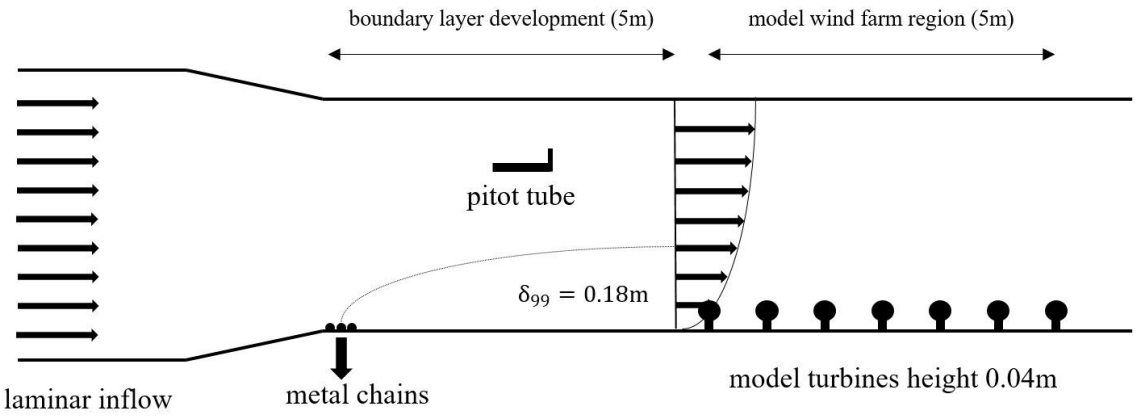

Figure 1 Schematic representation of the measurement set-up

Fitting 100 turbine models into the 1.2m wide wind tunnel at typically realistic spacing of S_x = 7D and S_y = 5D in the streamwise and cross-stream directions, respectively, where D is the turbine diameter, requires small turbine model diameters. We select D = 0.03m, which corresponds to a scaling factor of 1: 3,333 when compared to a full scale representative turbine of diameter 100m. Fabricating and operating rotating blades for such large number of small turbines

is not practical for our experiments. However, a porous disk model is capable of correctly characterizing the wake structure（Lignarolo et al., 2014）. Instead of extracting energy from the flow, a porous disk generates small-scale turbulence in the near wake. Thus, it acts like a momentum sink and also dissipating kinetic energy. Unlike rotating models which not only introduce tip and hub vortices but also rotational momentum and turbulence from the blades (Zhang et al., 2012), porous disk models produce near-wake by a grid. Since ambient velocity fluctuations in the atmospheric boundary layer have been shown have shown to effectively quickly overshadow any blade signatures and rotational momentum in the far wake (Aubrun et al., 2013), porous disk models have been proven to be effective in wind farm modeling in wind tunnels.

By measuring the thrust coefficient and the thrust force of each wind turbine, estimating the local wind speed at the porous disk model is possible. The equivalent wind turbine power then can be further estimated by momentum theory using standard relations, which will be described next. Still, using porous disks, measurements of high frequency characteristics of the power output is beyond reach. Basically, the thrust force is determined by measuring the amount of bending of the model tower with a strain gage fixed to every model tower. A strain gage (model Omega SGD-3/350-LY11) is attached to the “tower” as shown in Figure 2. And a half-bridge configuration with an Omega iNET-423

and iNET-555 acquisition device is used to dynamically collect measurement data. Assuming that the material properties remain relatively constant over time, the measured strain responds linearly to the resulting bending momentum of the tower where the strain gage is located (see Figure 3).

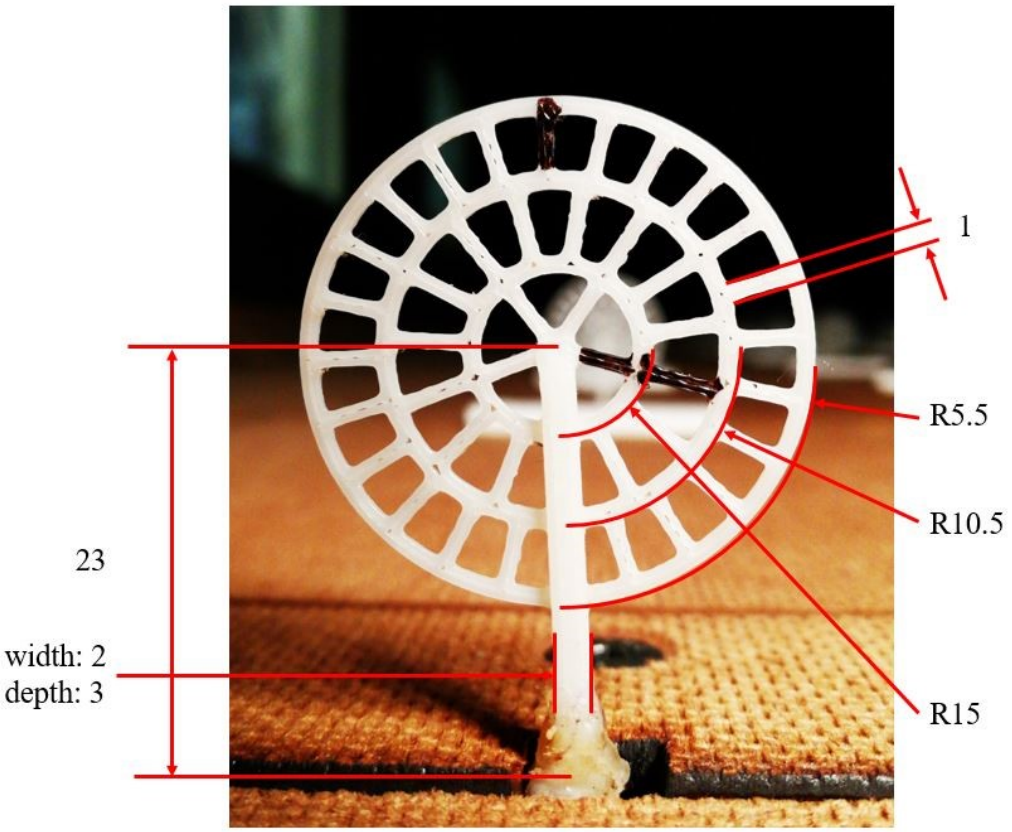

Figure 2 Photograph of the porous disk model. Dimensions are given in mm.

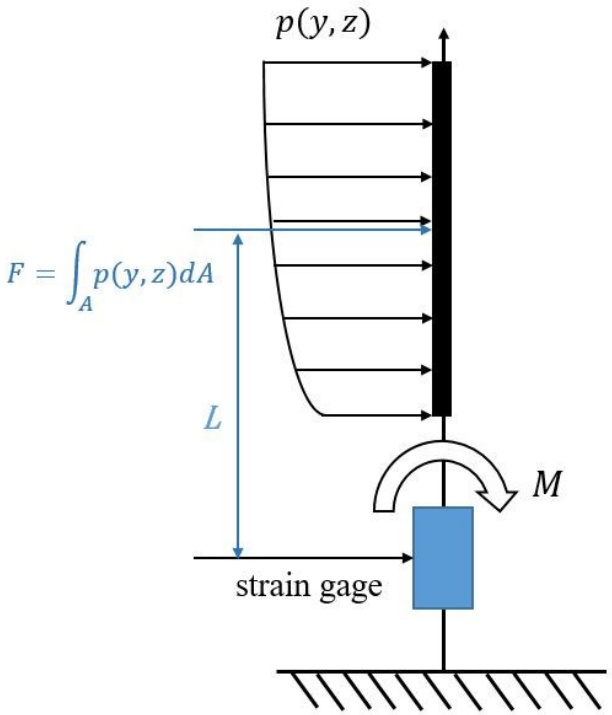

Figure 3 Schematic representation of the force distribution on the porous disk and the bending strain measurement by the strain gage.

Under static load and uniform load distribution situation, the bending moment of the model tower equals to the product of total thrust force multiplied by the distance between disk center and the strain gage center. Assume that this distance is represented by L and the load per unit area represented by $p(\mathrm{y},\mathrm{z})$. Then the instantaneous total thrust force is $F = \langle p \rangle A$, and the moment is given by

$$M = \int_A p(y,z) z dA = \langle p \rangle \langle z \rangle A = FL$$

The load distributions in our study are non-uniform, which means that the

center of the thrust force is no longer the center of the disk, but shifted a little. According to Bossuyt et al. (2017), this effect is taken into account by decomposing the force distribution in a spatially averaged component and spatially fluctuating component as follows.

$$p(y,z) = \langle p \rangle + \tilde{p}(y,z)$$

$$M = \langle p \rangle \langle z \rangle A + \int_A \tilde{p}(y,z) z dA$$

The second term of the right hand side of the static bending moment equation indicates the expected mean measurement error due to shear in the mean velocity profile. This static offset was estimated in Bossuyt et al. (2017) to be on the order of +4% using the incoming mean velocity profile and assuming a constant thrust coefficient over the disk. The thrust measurements of models of wind turbine models in the first row of the wind farm are corrected for this offset by multiplying the readings with a correction factor of 0.96. According to Chamorro and Porté-Agel (2011), the incoming velocity profile is significantly more uniform due to mixing in the wake for all downstream models. As a result, no correction is applied to turbines in subsequent rows.

Also as analyzed by Bossuyt et al. (2017), in a dynamic load situation, in which the thrust force fluctuates with the turbulent velocity field, the relation between bending moment measured by the strain gage and thrust on the disk is

more complicated. By modeling the structural response of the model as a harmonic oscillator using its first and dominant natural frequency, the dynamic thrust force behavior can be reconstructed from the strain measurements by using the equation,

$$F(t) = k\left(\frac{1}{\omega_n^2}\frac{d^2\varepsilon(t)}{dt^2} + 2\zeta\frac{1}{\omega_n}\frac{d\varepsilon(t)}{dt} + \varepsilon(t)\right)$$

where $\omega_n = \sqrt{k/m} = 2\pi f_n$. To this end, the natural frequency f_n, spring coefficient k and damping coefficient ζ are determined for every porous disk model from a static and dynamic calibration, allowing us to obtain measured values of the thrust force $F(t)$ from the measured strain time signal. With the thrust coefficient, the incoming spatially averaged velocity signal $\langle U\rangle(t)$ is reconstructed based on:

$$F(t) = \rho\langle U\rangle^2(t)C_T A/2$$

where $\mathrm{A} = \pi D^2/4$ is the rotor area. Then we get the expression:

$$\langle U\rangle(t) = \sqrt{\frac{2F(t)}{\rho C_T A}}$$

which represents the equivalent disc-averaged incoming velocity which would result in the same thrust force as measured. The reconstructed velocity allows us to estimate the equivalent power signal of the model as:

$$P(t) = \rho\langle U\rangle^3(t)C_P A/2$$

where C_P is the power coefficient. Note that the results to be presented in this paper focus on the ratio of turbine power to the power of the first row so that they are effectively independent of the actual power coefficient.

2.2 Roughness elements

A change from a smooth to a rough ground surface will increase the surface friction stress and consequently lead to a slow-down of wind above the surface. The increased shear will pass upwards through the surface layer until the wind throughout the entire boundary layer is slowed down. At that point the boundary layer returns to equilibrium with the surface. To reach equilibrium there must be a sufficiently long stretch of a given ground roughness. In such a condition, it is possible to still use a modified logarithmic law to describe the profile of the boundary layer. In this section we will use wind tunnel measurements to obtain a more intuitive view.

In this experiment we use fiber strips as roughness elements. They are placed transverse to the incoming flow and they span the wind tunnel width. To model the impact of buildings, woods and fence rows at a scale commensurate with that of real wind farm turbines, the height of the roughness elements must be properly scaled to the size of the wind turbine models. We assume that modern commercial wind turbines have an average diameter of 100 m, and typical heights of wind blocking roughness elements are about 10~20 m. For our model with a turbine diameter of 3

cm, the model roughness element should therefore be of a height of about 0.3~0.6 cm. Therefore, a 3/16 inch (approximately 0.47 centimeter) diameter braided polyester rope is chosen as a model roughness element for wind blockage in our micro wind farm model.

Figure 4 Photograph of the roughness elements applied to the micro wind farm in the wind tunnel

The boundary layer transition provoked by a rod-like roughness element can cause mean velocity fluctuations that are closely correlated with distance parallel to the ground (Tani & Sato, 1956). In order to ensure that the mean power output for each row of the model wind farm can equally reflect the impact from roughness elements, fiber stripes are placed with equal horizontal distance to model turbine rows. The layout of the transverse ropes is shown in Figure 4. A schematic representation is

shown in Figure 5. Two cases, where the roughness elements are placed only inside the wind farm region or where they are also placed upstream of the wind farm region with identical spacing as inside the wind farm area, are tested.

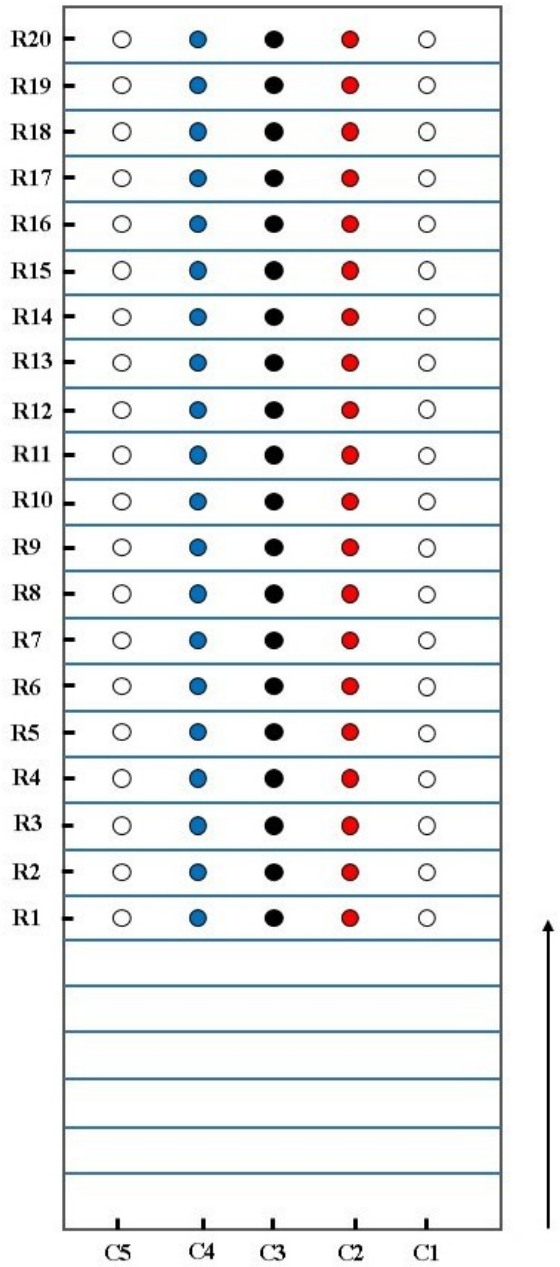

Figure 5 Schematic representation of the model wind farm layout with 5 columns in the streamwise direction and 20 rows in the spanwise direction. Roughness elements, represented by blue lines, are applied both inside and upstream of the wind farm model region. Vertical arrow indicates inflow direction.

2.3 Windbreaks

Among efforts trying to optimize the energy harvest efficiency of wind turbines by manipulating the interaction between the turbines and the atmospheric boundary layer, windbreaks is a relatively newly proposed methodology.

The local inviscid speedup above windbreaks applied to windfarms was predicted by Tobin and Chamorro (2017) in a way that is consistent with the method outlined in Tobin et al. (2017). The top-down model, which they applied in their study, has proven applicable in wind farm research topics such as the economic optimization of inter-turbine spacing (Meyers and Meneveau, 2012) and the impact of small vertical-axis turbines in large wind farms (Xie et al., 2017).

An increase in hub-height velocity was predicted when the windbreaks are ~2D or longer in the transverse direction compared to the turbine rotor diameters. The prediction was based on a perturbation of the two-dimensional Navier–Stokes Equations. Then the prediction of the power output of a wind turbine either with or without a windbreak, respectively represented as $\mathrm{P_{wb}}$ and $\mathrm{P_0}$, was obtained as follows:

$$\mathrm{P_{wb}} = \frac{1}{2} C_p \rho \pi D^2 [\bar{u}(z_h) + \Delta u]^3$$

$$\mathrm{P_0} = \frac{1}{2} C_p \rho \pi D^2 \bar{u}_0{}^3 (z_h)$$

where $\bar{u}_0$ is the estimate of hub-height velocity without windbreak effects. And

the value of Δu is dependent on the distance between the wind turbine and the windbreak.

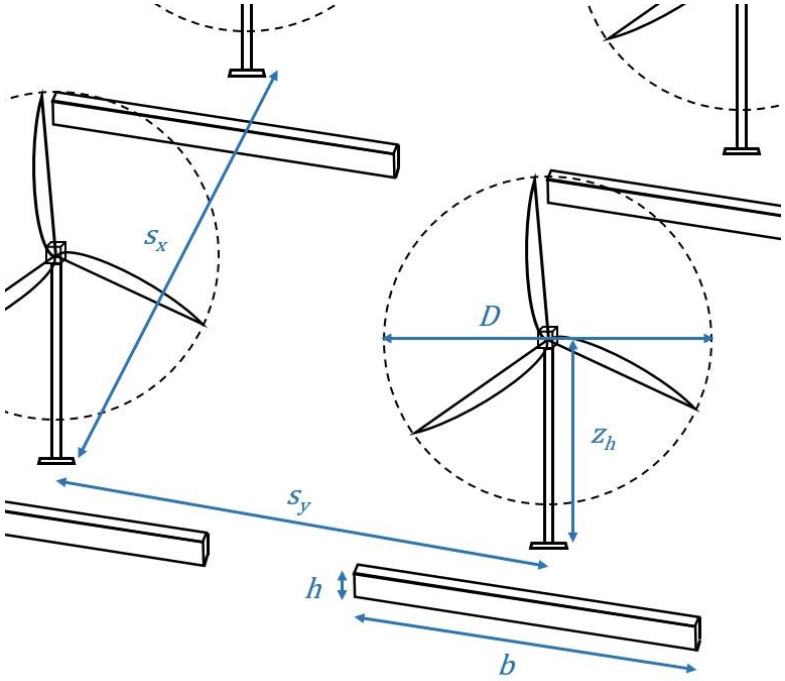

Figure 6 Conceptual schematic of the layout of an infinite wind farm with windbreaks in research of Tobin and Chamorro (2017)

In their research, Tobin and Chamorro (2017) also used large-eddy simulations (LES) to make predictions of turbine power output using an approach based on a neutrally stratified boundary layer driven by a streamwise body force. Both the wind turbines and windbreaks were modelled as porous regions using the actuator disk method. An infinite array of wind turbines with rotor diameter $\mathrm{D} = 100\mathrm{m}$ and hub height $z_h = 100m$, spaced S_x and S_y in the streamwise and transverse directions was considered. A windbreak of height h and transverse width b was also placed facing the

direction of mean flow a short distance ($\sim 5h$) upwind of each turbine. A schematic of the concept is shown in Figure 6.

To reproduce this result by wind tunnel measurements, we set up windbreaks with similar geometry features in the same model wind farm as used in roughness elements measurements. The wind farm remains a streamwise spacing of S_x = 7D and spanwise spacing of S_y = 5D with D representing turbine model diameter of 0.03m. Tobin and Chamorro (2017) used a windbreak height of $h = 12$ m and 20 m in their simulations. This results in a model windbreak height of h =0.0036~0.006 m under the assumption that commercial wind turbine diameters average 100 meters. Therefore, a plastic corrugated sheet was chosen as the raw material for manufacturing windbreak models. For a windbreak width of ~2D used in the LES, the same relative length scale was used here, i.e. $b = 0.06$ m. Models were fixed to the wind tunnel floor using mounting tapes adding up to total height of 0.0048 m, which is acceptable for present purposes. Also, a distance of $\sim 5\mathrm{h} = 0.024$ m is set from the leading edge of the windbreak model to the wind turbine model. A total of 100 windbreaks were installed, each in front of a porous disk model to simulate the implementation of windbreaks to large-scale wind farms. Photographs of the implemented windbreaks are shown in Figures 7 and 8.

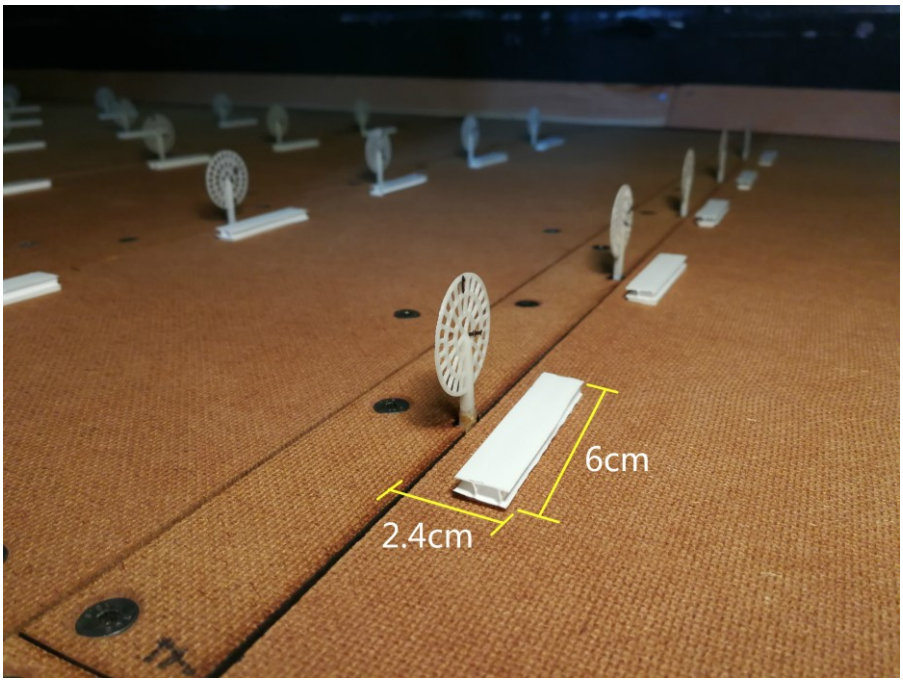

Figure 7 Detailed photograph of windbreaks applied to porous disk models.

Dimensions are marked.

Figure 8 Overview photograph of windbreaks applied to micro wind farm in the

wind tunnel

3. Results and Discussion

The measurement capabilities of the designed micro wind farm are demonstrated with wind tunnel measurements integrating data from 60 turbine models within a 100-turbines model wind farm. The data acquisition method is described in §3.1. The mean row power performance with the application of roughness elements is discussed in §3.2. The mean row power performance with the application of windbreaks is discussed in §3.3.

3.1 Data acquisition

Measurements are performed for both the roughness elements and windbreaks cases.

Strain signals are measured with the Omega iNET-423 voltage input cards and the Omega iNET-430 16bit A/D converter, which use high frequency noise reduction based on internal 4kHz low-pass filterings. The sampling frequency for each model is limited to 0.866kHz because of the large number of simultaneous strain gage measurements. However, measurements for a single model have shown that the aliasing error is small for a frequency range of 0-200Hz (Bossuyt et al., 2017). This covers our range of interest. The data acquisition measurement time for each case was approximately 10 minutes.

Linear creep correction is done by correcting with the remaining strain at the end

of the measurement period after the wind tunnel is turned off. This correction is typically on the order of 4%.

To keep the inflow wind speed as a controlled variable, the rotor speed of the wind tunnel was manipulated through a dial controller. The wind speed inside the wind tunnel was precisely monitored through a pitot tube, which is installed above the wind tunnel floor with a position marked in Figure 1. Multiple measurements proved that under equal rotor speed, the inflow wind speed differences caused by application of roughness elements or windbreaks is negligible. Hence, in order to make comparisons, a constant rotor speed is maintained to keep a constant inflow wind speed for all measurements.

3.2 Mean power measurements for two roughness elements cases

Figure 9 shows the measured normalized baseline power output for an aligned layout, calculated from the strain signal data. No ground surface modifications are applied to the wind farm in this case. The mean power is normalized by the power of the first row. The different symbols indicate individual porous disk models for various columns. The mean row power shows good agreement with the classical trend seen for aligned wind farms: the power decreases significantly in the first two to three rows after which the power deficit becomes approximately constant. The drop in power of 50% from first row is consistent with measurements for the Horns Rev wind farm

shown in Figure 4.2 of M´echali et al. (2006). Measurement uncertainties connected to the absolute quantities and the need to average over multiple models per row are illustrated by variations within each row.

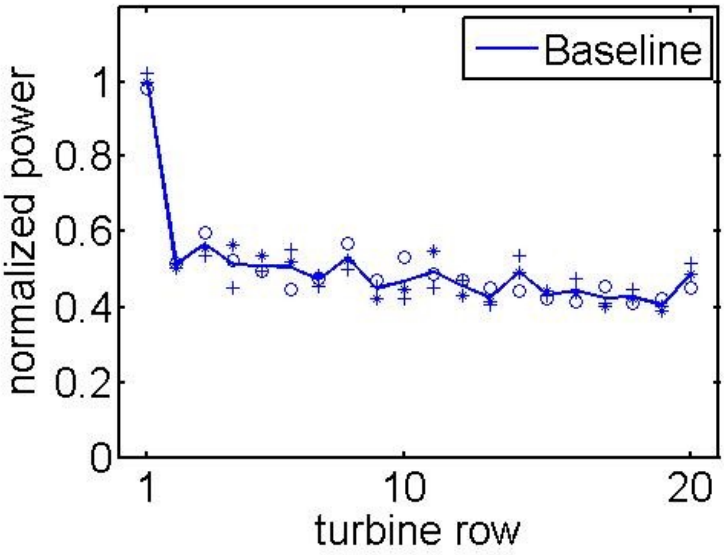

Figure 9 Mean row power measured by porous disk models for baseline case. The different symbols indicate individual porous disk models for various columns.

Figure 10 shows a measured power output comparison between the baseline case and the roughness elements case with roughness elements applied both inside and upstream of the wind farm model region, as shown schematically in Figure 5. Strips with constant spacing are extended to the horizontal position of the pitot tube. To directly observe the impact from roughness elements, the mean row power of roughness elements case is also normalized by mean row power of the first row of baseline measurement. From the plot we can observe a mean row power deficit of 35%

at the first row and generally a constant level of around 25% for the following rows. This result, that hub-height wind speed (reflected here by the mean row power), is reduced downstream of surface-attached rods, agrees well with the conclusions from research investigating boundary-layer modification by roughness elements (Tani & Sato, 1956).

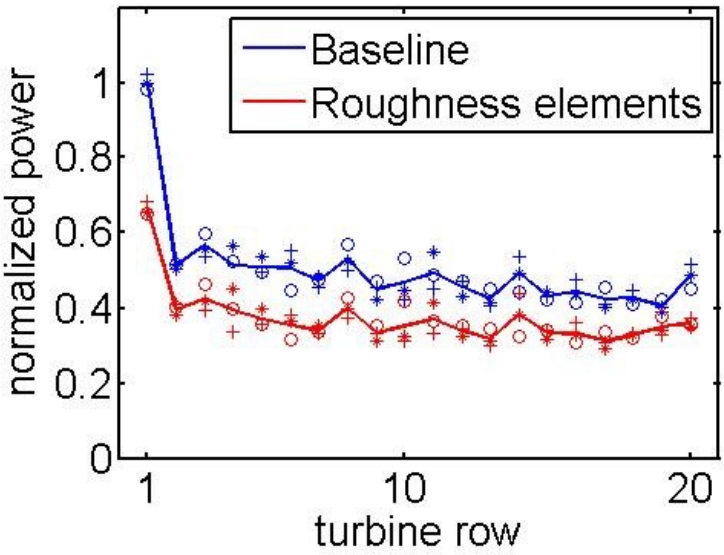

Figure 10 Mean row power comparison between measured baseline case and the roughness element case with roughness elements applied both inside and upstream of the micro wind farm model region, as shown in Figure 5.

Figure 11 shows a measured power output comparison between the baseline case and the roughness elements case where roughness elements are only applied inside the model wind farm region. The absence of roughness elements upstream of the wind farm thus creates upstream conditions that are equal to those of the baseline

measurement case. This case is schematically shown in Figure 12. In Figure 11 the power of the roughness elements case is also normalized by the mean row power of the first row of the baseline measurement. For the following rows, we can observe a significant power deficit that increases from row two to row seven, after which the power deficit basically remains at the same level. Figure 13 shows the combined measurement results of the baseline case and both roughness elements cases. As can be seen, the mean row power deep inside the array, here from row eight to row twenty are quite similar between the two roughness elements cases. However, the inflow roughness of the second roughness case has a noticeable impact on the mean power until row 7. This observation indicates that the formation of a new fully developed mean velocity profile requires a certain distance downstream of the ground roughness transition and that it depends on the level of inflow roughness.

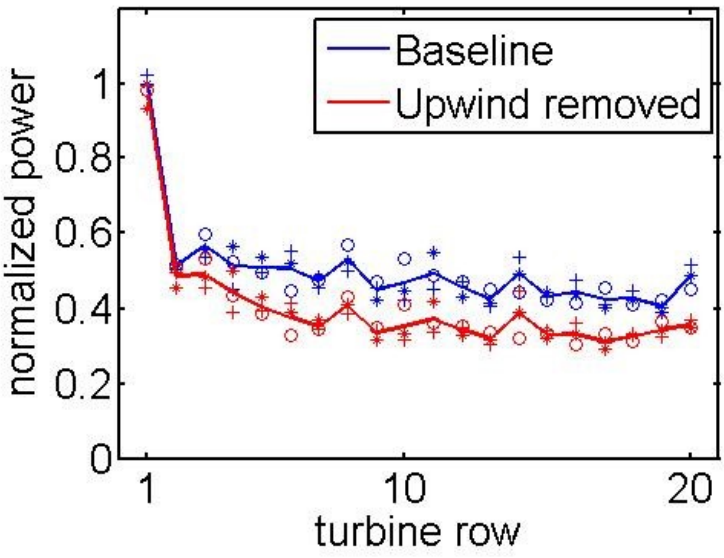

Figure 11 Mean row power comparison between measured baseline case and roughness element case without roughness elements upstream of the micro wind farm model.

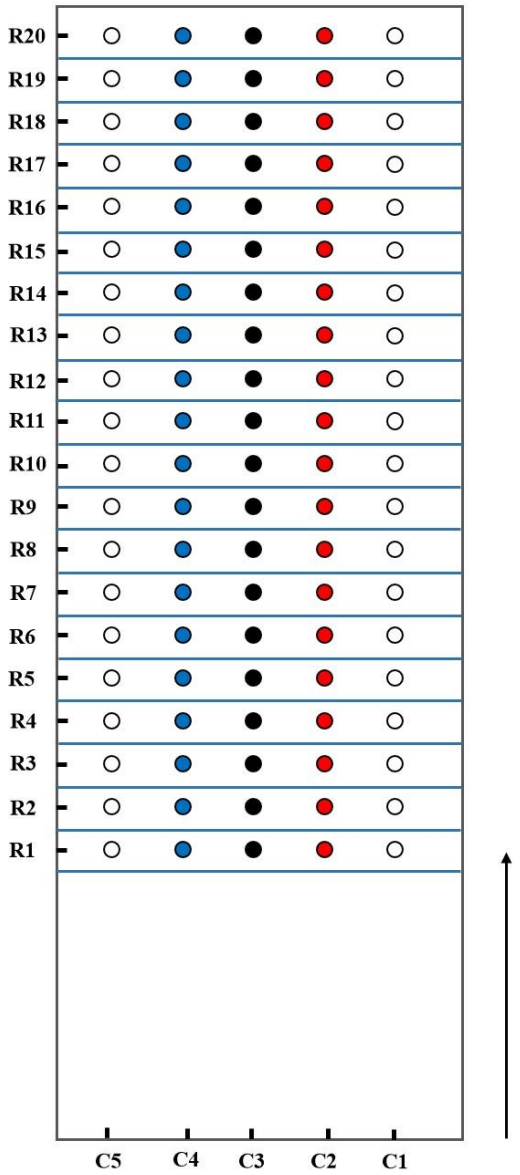

Figure 12 Schematic representation of the model wind farm layout with roughness elements only applied inside the micro wind farm model region. Vertical

arrow indicates inflow direction.

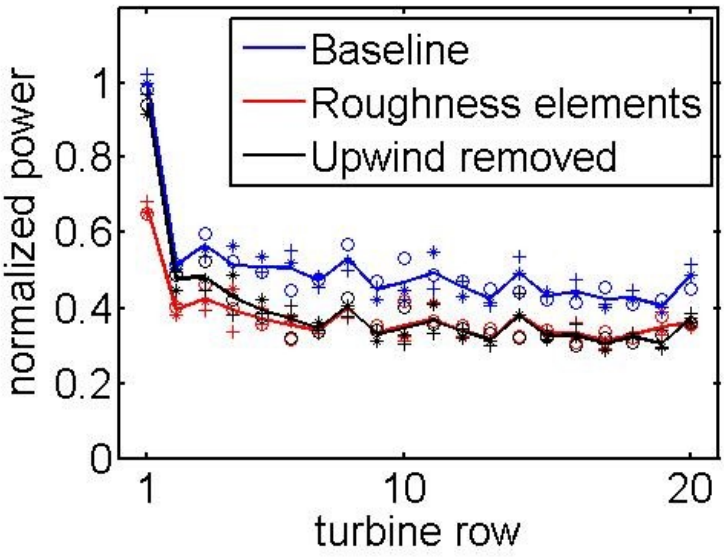

Figure 13 Mean row power comparison between measured baseline case, roughness elements case with and without roughness elements applied upstream of the micro wind farm model.

3.2 Mean power measurements for the windbreaks case

Figure 14 shows a comparison between the measured power output of the baseline case and the windbreaks case with windbreaks applied to each of the 100 porous disk models within the model wind farm with the aligned layout. To directly observe the impact from windbreaks, the mean row power results of the windbreaks case is normalized by the mean row power of the first row of the baseline measurement. A small power deficit is observed at the first row showing that already

for the first row in this case the windbreaks do not appear to increase power. Also, further downstream in the wind farm we observe a general 5%~10% power deficit compared to the baseline case. The two cases agree with the classical trend seen for aligned wind farms: the power decreases significantly in the first two to three rows after which the power deficit becomes approximately constant.

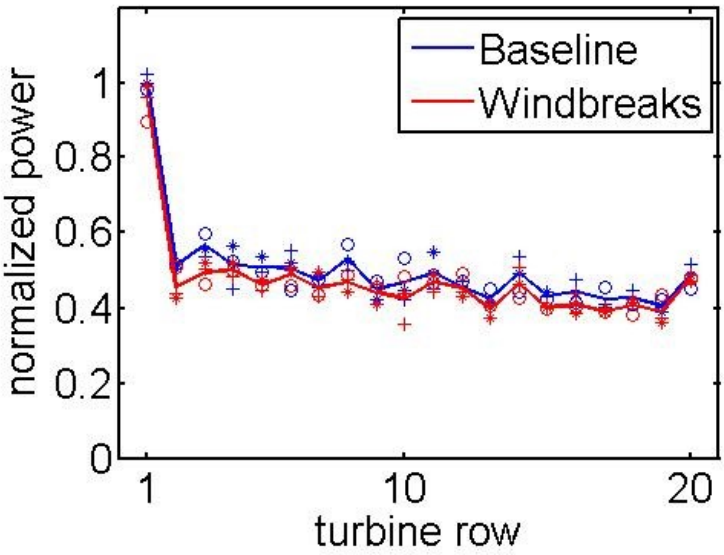

Figure 14 Mean row power comparison between measured baseline case and windbreaks case

From basic fluid dynamics in wind farms it can be expected that the combined impacts of the inviscid speed-up from flow over windbreaks and the enhanced mixing and greater velocity deficits in their wakes is strongly dependent on the details of the wind farm layout. Therefore, the applicability of windbreaks in wind farms may not be universal and present results may not be applicable to all layouts. Model

predictions such as those developed by Tobin and Chamorro (2017), who augmented the top-down model with roughness effects of windbreaks and the induced flow speed-up in a combined simulation, can provide useful additional information to compare our present results. Top-down model calculations and large-eddy simulation data shown in Figure 5 of Tobin and Chamorro (2017) for aligned layout at h/z_{hub} = 4.8mm/23mm $\approx$ 0.2, prediction made with top-down model indicates a 25% power reduction at $S_x = 6D$, i.e. no increase. Moreover, their LES results suggest even larger power reductions, about 35%. It is clearly observed from their Figure 5 that no positive windbreaks effect is expected with S_x less than 50 times D. Therefore, present wind tunnel measurements agree well with their results, suggesting that the net impact of windbreaks on power output for most realistic wind farm spacings is negative and not worth pursuing in practical implementations of wind energy. For further studies, wind tunnel measurements investigating effects of windbreaks in wind farms with larger wind turbine spacings may be needed.

4. Conclusions

An experimental wind tunnel study of ground surface effects, including roughness elements and windbreaks, on a model wind farm has been carried out. The model wind farm contains 100 porous disk wind turbine models arranged in a 5×20 aligned layout. The 3×20 model turbines in the center three columns are

instrumented with strain gages from which time dependent thrust force has been acquired and recorded. Power output for each wind turbine model was deduced from calibrated and processed strain signals.

Strip-like roughness elements with height of 4.7 mm and spacing of 7 times turbine diameter, which is equal to streamwise turbine row spacing, were uniformly applied inside the model wind farm region and upstream of the model wind farm region. Baseline measurements - without surface roughness modification were performed. The mean row power results show good agreement with results for the Horns Rev wind farm (Méchali et al., 2006) and many other power measurements and simulations in aligned wind farms.

Compared to baseline measurement, a mean row power deficit of 35% at the first row and generally around 25% at following rows was observed for the first roughness elements case considered, in which an upstream fetch also included roughness elements. This result agrees well with the research investigating boundary-layer modifications by roughness elements (Tani & Sato, 1956). With the roughness elements upstream of the wind farm removed, the mean row power of the first row remains the same as in the reference case, and then decreases and approaches that of the prior case after the seventh row of turbines, i.e. deep inside the windfarm. Identical power deficit results were obtained from row eight to row twenty for both roughness elements cases, i.e. the results became independent of whether roughness

elements were either applied or not applied upstream of wind farm. These results provide information about the effects of upstream roughness on the development length of conditions inside the windfarm.

The measurement result of windbreaks case shows a small power reduction at the first row and a general 5%~10% power reduction at following rows compared to the baseline measurements. These results agree with the conclusions gained from the top-down model predictions and LES results from Tobin and Chamorro (2017), who deduced a negative net impact of windbreaks in large wind farms. The current results confirm their findings that windbreaks are unlikely to work in realistic windfarm conditions.

Bibliography

Ackermann, T., Söder, L., An overview of wind energy-status 2002, In Renewable and Sustainable Energy Reviews, Volume 6, Issues 1–2, 2002, Pages 67-127, ISSN 1364-0321, https://doi.org/10.1016/S1364-0321(02)00008-4.

Aubrun, S., Loyer, S., Hancock, P., Hayden, P.: Wind turbine wake properties: Comparison between a nonrotating simplified wind turbine model and a rotating model. Journal of Wind Engineering and Industrial Aerodynamics 120, 1 – 8 (2013)

Blom, J. and L. Wartena, 1969: The Influence of Changes in Surface Roughness on the Development of the Turbulent Boundary Layer in the Lower Layers of the Atmosphere. J. Atmos.

Sci., 26, 255-265, https://doi.org/10.1175/1520-0469(1969)026<0255:TIOCIS>2.0.CO;2

Bossuyt, J., Howland, M.F., Meneveau, C. et al.: Measurement of unsteady loading and power output variability in a micro wind farm model in a wind tunnel. Exp Fluids (2017) 58: 1. https://doi.org/10.1007/s00348-016-2278-6

Chamorro, L. P. and Port´e-Agel, F., "Turbulent flow inside and above a wind farm: a wind-tunnel study," Energies 4, 1916–1936 (2011).

Chamorro, L.P. & Porté-Agel, F. Boundary-Layer Meteorol (2009) 132: 129. https://doi.org/10.1007/s10546-009-9380-8

De Paepe, W., Pindado, S., Bram, S., Contino, F., Simplified elements for wind-tunnel

measurements with type-III-terrain atmospheric boundary layer, In Measurement, Volume 91, 2016, Pages 590-600, ISSN 0263-2241, https://doi.org/10.1016/j.measurement.2016.05.078.

Deal, W. F., Wind power: an emerging energy resource. Technology and Engineering Teacher, 9 (2010), pp. 9-15

Dong, Z.; Luo, W.; Qian, G.; Wang, H. A wind tunnel simulation of the mean velocity fields behind upright porous fences. Agric. For. Meteorol. 2007, 146, 82–93.

Essa, K. S. M., Embaby, M., & Etman, S. M. (2003). A notional variation of the wind profile power-law exponent as a function of surface roughness and stability. In 4th Conference on nuclear and particle physics. Fayoum, Egypt.

Hand M, Simms D, Fingersh L, Jager D, Cotrell J, Schreck S, Larwood S. Unsteady aerodynamics experiment phase vi: Wind tunnel test configurations and available data campaigns. Technical report NREL/TP-500-29955, NREL, December 2001.

Irwin, J. (1979). A theoretical variation of the wind profile power-law exponent as a function of surface roughness and stability. Atmospheric Environment (1967). 13. 191-194. 10.1016/0004-6981(79)90260-9.

Iungo, G. V., Experimental characterization of wind turbine wakes: Wind tunnel tests and wind LiDAR measurements, In Journal of Wind Engineering and Industrial Aerodynamics, Volume 149, 2016, Pages 35-39, ISSN 0167-6105, https://doi.org/10.1016/j.jweia.2015.11.009

Jiménez, J. “Turbulent flows over rough walls,” Annu. Rev. Fluid Mech. 36, 173 (2004). https://doi.org/10.1146/annurev.fluid.36.050802.122103

Judd, M.J., Raupach, M.R. & Finnigan, J.J. Boundary-Layer Meteorol (1996) 80: 127. https://doi.org/10.1007/BF00119015

Krogstad, P.Å., Eriksen P.E., 2013. “Blind test” calculations of the performance and wake development for a model wind turbine. *Renew. Energy* 50:325–33

Krogstad, P. Å., Sætran, L., Adaramola, M.S., 2015. “Blind test 3” calculations of the performance and wake development behind two in-line and offset model wind turbines. *J. Fluids Struct.* 52:65–80

Leung, D.Y.C. & Yang, Y. Wind energy development and its environmental impact: A review, In Renewable and Sustainable Energy Reviews, Volume 16, Issue 1, 2012, Pages 1031-1039, ISSN 1364-0321, https://doi.org/10.1016/j.rser.2011.09.024.

Lignarolo, L., Ragni, D., van Bussel, G., et al.: Kinetic energy entrainment in wind turbine and actuator disc wakes: an experimental analysis. In: Journal of Physics: Conference Series, vol. 524, p. 012163. IOP Publishing (2014)

M´echali, M., Barthelmie, R., Frandsen, S., Jensen, L., R´ethor´e, P.E.: Wake effects at horns rev and their influence on energy production. In: Proceedings of the European Wind Energy Conference and Exhibition. Citeseer (2006)

Mattuella, J.M.L., Loredo-Souza, A.M., Oliveira, M.G.K., Petry, A.P., Wind tunnel

experimental analysis of a complex terrain micrositing, In Renewable and Sustainable Energy Reviews, Volume 54, 2016, Pages 110-119, ISSN 1364-0321, https://doi.org/10.1016/j.rser.2015.09.088.

Meyers, J.; Meneveau, C. Optimal turbine spacing in fully developed wind farm boundary layers. Wind Energy 2012, 15, 305–317.

Nickerson, E.C., Smiley, V. E., 1975, Surface layer and energy budget parameterizations for mesoscale models, Jour. Appl. Meteor., 14. 297-300

Pierella, F., Krogstad P.Å., Sætran, L., 2014. Blind test 2 calculations for two in-line model wind turbines where the downstream turbine operates at various rotational speeds. *Renew. Energy* 70:62–77

Stevens, R. J., Meneveau, C. "Flow structure and turbulence in wind farms", *Annual Review of Fluid Mechanics*, vol. 49, no. 1, 2017.

Ragheb, M (2012) Wind Shear, Roughness Classes and Turbine Energy Production. Available at: https://netfiles.uiuc.edu/mragheb (Accessed: 14 August 2012)

Schepers, J., Boorsma, K., Cho, T., Gomez-Iradi, S., Schaffarczyk, P., et al. 2012. Final report of IEA Task 29, Mexnext (phase 1): analysis of MEXICO wind tunnel measurements. Rep. ECN-E12-004, ECN, Amsterdam

Schepers, J.G., Boorsma, K., Gomez-Iradi, S., Schaffarczyk, P., Madsen, H.A., et al. 2014. *Final report of IEA Wind Task 29: Mexnext (Phase 2)*. Rep. ECN-E14-060, ECN, Amsterdam

Simms, D., Schreck, S., Hand, M., Fingersh, L., NREL unsteady aerodynamics experiment in the NASA-Ames wind tunnel: a comparison of predictions to measurements. NREL/TP-500-29494. Colorado, USA: National Renewable Energy Laboratory; 2001. p. 1*e*44

Tani, I., Sato, H., Boundary-Layer Transition by Roughness Element, Journal of the Physical Society of Japan, 11, 1284-1291 (1956) 10.1143/JPSJ.11.1284

Tobin, N. and Chamorro, L. P. (2017). Windbreak effects within infinite wind farms. Energies 2017, 10(8), 1140; doi:10.3390/en10081140

Tobin, N., Hamed, A.M., Chamorro, L.P. Fractional Flow Speed-Up from Porous Windbreaks for Enhanced Wind-Turbine Power. Bound.-Lay. Meteorol. 2017, 163, 253–271, doi:10.1007/s10546-016-0228-8.

Xie, S.; Archer, C.L.; Ghaisas, N.; Meneveau, C. Benefits of collocating vertical-axis and horizontal-axis wind turbines in large wind farms. Wind Energy 2017, 20, 45–62.

Zhang, W., Markfort, C., Port´e-Agel, F.: Near-wake flow structure downwind of a wind turbine in a turbulent boundary layer. Experiments in Fluids 52(5) (2012)

Zhang, W., Markfort, C.D. & Porté-Agel, F. Boundary-Layer Meteorol (2013) 146: 161. https://doi.org/10.1007/s10546-012-9751-4

Biography

Yifan Zhang was born in 1994 in China.

Yifan did his undergraduate work at Zhejiang University, Hangzhou, China where he majored in Energy Engineering and minored in English.

In 2016, Yifan began his masters at Johns Hopkins University. He was a teaching assistant for Charles Meneveau's Heat Transfer class.